Power flow through multidimensional compliant joints using mobility and modal approaches

Todd E. Rook and Rajendra Singh
Acoustics and Dynamics Laboratory, Department of Mechanical Engineering, The Ohio State University, 206 West 18th Avenue, Columbus, Ohio 43210-1107

(Received 1 July 1994; revised 30 November 1994; accepted 5 January 1995)

An analytical framework, based on the refinements to the mobility and modal approaches, is proposed to calculate the structural power flow through multidimensional compliant joints or connections. The built-up assembly is divided into the classical model of a noise control problem, i.e., source, path (joint), and receiver. Both methods place emphasis on the joint properties and account for different paths and mechanisms of noise transmission (e.g., forces and moments). Only the discrete system formulation is considered and results obtained via exact (unsynthesized) and the proposed component synthesis procedures perfectly match with each other. The mobility method is found to be useful for distinguishing which path (joint) transmits power and the complementary modal method yields information on the newly defined modal dissipation efficiencies. Finally the issues of scalar versus vector joints and rigid versus compliant connections are addressed by using a pedagogical example of a 10 degrees-of-freedom system.

PACS numbers: 43.40.Hb

INTRODUCTION

A. Motivation

Machines and equipment are often built-up assemblies of many components and subassemblies joined together via bolts, rivets, gaskets, or welded connections. The dynamics of the assembled system is often affected by the compliance and damping of the joints or connections.[1,2] Nonetheless, prior modeling efforts[1–8] in the calculation of either modal solutions or vibratory power flows have assumed the joints to be either rigid or scalar springs. In some cases,[9] the analysis is terminated at the joint as if it were assumed to be a boundary condition (fixed, free, or simply supported). Since the literature in this area is rather sparse, a definite need exists to establish a mathematical framework for including joints in a systematic manner for the calculation of modal data, transfer functions, and vibratory power flows. While many joints and machine elements are inherently nonlinear, only linear time-invariant characteristics over the lower frequency regime are considered here as a logical first step.

Yet another important research issue is the dimension of the joint. An example of this is the situation in which both the force and moment transmissions through a joint are significant.[4–8] Although moment paths may be negligible at lower frequencies,[10] some studies suggest otherwise.[11] For the sake of simplifying formulations, several prior studies have used scalar connections,[3] but for realistic joints, vector transmission paths must be considered; that is the focus of this study. Intended applications of the theory presented in this article include sheet metal structures with joints and rotating machines where bearings may be thought of as joints from the standpoint of vibration transmission phenomenon. Given the complexity of real-life problems, numerical and experimental methods must often be employed, and therefore a discretized system model or database is assumed to be available.

B. Objectives

Several existing narrow-band analysis methods a the form of component synthesis procedures, thereby a ing better examination of the consequences of design fications to a particular substructure or component. M these procedures either synthesize components in the domain[4] or the frequency domain.[5,6,12–15] Since none existing methods is believed to be fully capable of ac ing the issues associated with multidimensional cor joints, we extend and refine two established narro analysis procedures. One method is based on a mobil proach similar to those in Refs. 5, 6, 12, and 13. The based on a modal synthesis approach such as method,[16] where proportional damping is assumed su all the modes are real-valued. In our study, the ass structure is decomposed into three key components form of a classical noise control problem, as shown 1(a). The source structure (s) contains the origin narrow-band vibrational energy (excitation), and is active component. The next component represents th less, nonconservative, and nonrigid connections or jc which may be multidimensional and connect the a structures at several discrete locations. From the jc power is then transmitted to the passive receiver (c), which for the sake of convenience can be furthe posed into free receiver (a) and foundation (b) con Often the foundation component may be modeled eralized termination impedance[17] or energy sink.

I. ANALYTICAL FORMULATION

A. Mobility approach

Similar to the electrical "black box" procedures,[18,19] this approach is not concerned w ternal behavior of the components. Rather it onl the interfacial structural mobilities **Y**, forces **F**, a

 0001-4966/95/97(5)/2882/10/$6.00

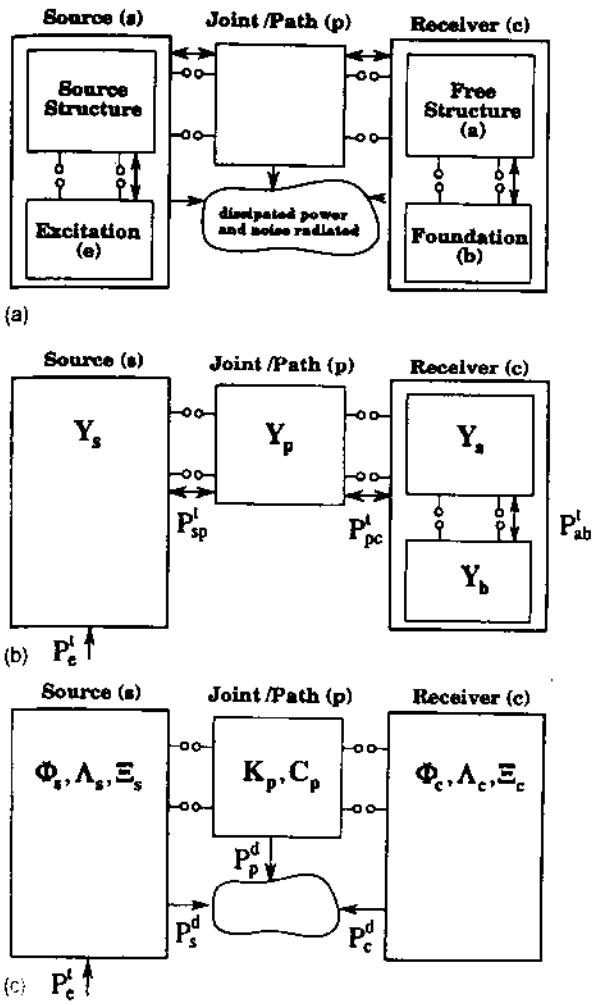

FIG. 1. Schematic of the proposed method. (a) General component notation. (b) Notation for mobility approach. (c) Notation for modal approach.

ties v as shown in Fig. 1(b). Here bold symbols denote matrices or vectors of dimension n, since we are interested in vector rather than scalar paths. In our analysis, the mobility matrix assumes free–free boundary conditions on each component. When studying multiple connections with mobility approaches, many investigators have neglected the transfer mobilities to simplify the problem.[20,21] Such an approximation serves to uncouple the joint locations so that only point mobilities may be used, but it is not really applicable at the lower frequencies in which we are particularly interested. Consequently the full component mobility matrices including transfer mobilities are retained in this study. For the narrow-band analysis, we first define the following equations in the frequency domain (ω), with reference to Fig. 1(b):

$$\begin{Bmatrix} \mathbf{v}_e(\omega) \\ \mathbf{v}_{sp}(\omega) \end{Bmatrix} = \begin{bmatrix} \mathbf{Y}_s^{11}(\omega) & \mathbf{Y}_s^{12}(\omega) \\ \mathbf{Y}_s^{21}(\omega) & \mathbf{Y}_s^{22}(\omega) \end{bmatrix} \begin{Bmatrix} \mathbf{F}_e(\omega) \\ -\mathbf{F}_{sp}(\omega) \end{Bmatrix}, \tag{1a}$$

$$\begin{Bmatrix} \mathbf{v}_{pa}(\omega) \\ \mathbf{v}_{ab}(\omega) \end{Bmatrix} = \begin{bmatrix} \mathbf{Y}_a^{11}(\omega) & \mathbf{Y}_a^{12}(\omega) \\ \mathbf{Y}_a^{21}(\omega) & \mathbf{Y}_a^{22}(\omega) \end{bmatrix} \begin{Bmatrix} \mathbf{F}_{pa}(\omega) \\ -\mathbf{F}_{ab}(\omega) \end{Bmatrix}, \tag{1b}$$

$$\begin{Bmatrix} \mathbf{v}_{sp}(\omega) \\ \mathbf{F}_{sp}(\omega) \end{Bmatrix} = \begin{bmatrix} \mathbf{I} & \mathbf{Y}_p(\omega) \\ \mathbf{0} & \mathbf{I} \end{bmatrix} \begin{Bmatrix} \mathbf{v}_{pa}(\omega) \\ \mathbf{F}_{pa}(\omega) \end{Bmatrix}, \tag{1c}$$

$$\mathbf{v}_{ab}(\omega) = \mathbf{Y}_b(\omega)\mathbf{F}_{ab}(\omega), \tag{1d}$$

where $\mathbf{I}$ is the identity matrix and the superscripts 11, 12, 21, and 22 denote the submatrices for the input (1) and output (2) ports/interfaces of a component. Furthermore, $\mathbf{v}_e$ is the velocity vector at the excitation (e) interface of dimension n_e, $\mathbf{v}_{sp}$ is that of the source (s)–joint (p) interface of dimension n_p, $\mathbf{v}_{pa}$ is that of the joint (p)–free receiver (a) interface also of dimension n_p and $\mathbf{v}_{ab}$ is that of the free receiver (a)–foundation (b) interface of dimension n_b; the interfacial force vectors are defined analogously. We should point out that the method is generic enough to accept n_e uncorrelated excitations, but we will only consider a single excitation in this study for the sake of clarity. Consequently, $\mathbf{Y}_s$ is of dimension n_e+n_p, $\mathbf{Y}_a$ is of dimension n_b+n_p, $\mathbf{Y}_p$ is of dimension n_p, and $\mathbf{Y}_b$ is of dimension n_b. The joints are considered massless, and are therefore only characterized by their stiffness, $\mathbf{K}_p$, and damping , $\mathbf{C}_p$, matrices which are of dimension n_p and are assumed symmetric for the sake of convenience. Our assumptions of massless and discrete joints are valid for lower frequencies, and are consistent with the specification of a narrow-band approach such as the mobility/receptance methods.[5,6,12,13] Note that to avoid using a singular mobility matrix of dimension $2n_p$ in Eq. (1c), the joints' equations are posed in the form of a transfer matrix with a nonsingular $\mathbf{Y}_p = i\omega(\mathbf{K}_p + i\omega\mathbf{C}_p)^{-1}$ of dimension n_p. Couplings between degrees of freedom are permitted by these general connections; each joint may be represented by a 6×6 matrix (which may then be reduced further in dimension depending on symmetries and type of joint). Rearranging the equations in (1) by equating the velocities, and utilizing the fact that the massless joint has the same force magnitude at its input and output, i.e., $\mathbf{F}_{sp} = \mathbf{F}_{pa} = \mathbf{F}_p$, yields the following matrix form:

$$\begin{bmatrix} \mathbf{Y}_a^{11}(\omega) + \mathbf{Y}_s^{22}(\omega) + \mathbf{Y}_p(\omega) & -\mathbf{Y}_a^{12}(\omega) \\ -\mathbf{Y}_a^{21}(\omega) & \mathbf{Y}_a^{22}(\omega) + \mathbf{Y}_b(\omega) \end{bmatrix} \begin{Bmatrix} \mathbf{F}_p(\omega) \\ \mathbf{F}_{ab}(\omega) \end{Bmatrix} = \begin{bmatrix} \mathbf{Y}_s^{21}(\omega) \\ \mathbf{0} \end{bmatrix} \mathbf{F}_e(\omega), \tag{2}$$

which we wish to solve for the interfacial forces, $\mathbf{F}_p$ and $\mathbf{F}_{ab}$. The inversion of the matrix can be done in terms of the submatrices;[19] this is desirable to economize the method since all operations are then performed on the smaller component matrices thereby eliminating the need to numerically assemble them. This process results in the following equation:

$$\begin{Bmatrix} \mathbf{F}_p(\omega) \\ \mathbf{F}_{ab}(\omega) \end{Bmatrix} = \begin{bmatrix} \mathbf{\Gamma}_2(\omega) \\ \mathbf{\Gamma}_1(\omega)\mathbf{\Gamma}_2(\omega) \end{bmatrix} \mathbf{F}_e(\omega), \tag{3a}$$

where the intermediate matrices are given by

$$\mathbf{\Gamma}_1(\omega) = (\mathbf{Y}_a^{22}(\omega) + \mathbf{Y}_b(\omega))^{-1}\mathbf{Y}_a^{21}(\omega), \tag{3b}$$

$$\mathbf{\Gamma}_2(\omega) = [(\mathbf{Y}_a^{11}(\omega) + \mathbf{Y}_s^{22}(\omega) + \mathbf{Y}_p(\omega)) - \mathbf{Y}_a^{12}(\omega)\mathbf{\Gamma}_1(\omega)]^{-1}\mathbf{Y}_s^{21}(\omega). \tag{3c}$$

The previous equation may then be augmented with the excitation, $\mathbf{F}_e$, so that all the interfacial forces are now defined as

$$\begin{Bmatrix} \mathbf{F}_e(\omega) \\ \mathbf{F}_p(\omega) \\ \mathbf{F}_{ab}(\omega) \end{Bmatrix} = \begin{bmatrix} \mathbf{I} \\ \boldsymbol{\Gamma}_2(\omega) \\ \boldsymbol{\Gamma}_1(\omega)\boldsymbol{\Gamma}_2(\omega) \end{bmatrix} \mathbf{F}_e(\omega). \tag{4}$$

Furthermore, the interfacial velocities may be obtained from these interfacial forces through the following equation that arises from rearranging Eq. (1);

$$\begin{Bmatrix} \mathbf{v}_e(\omega) \\ \mathbf{v}_{pa}(\omega) \\ \mathbf{v}_{ab}(\omega) \end{Bmatrix} = \begin{bmatrix} \mathbf{Y}_s^{11}(\omega) & -\mathbf{Y}_s^{12}(\omega) & \mathbf{0} \\ \mathbf{0} & \mathbf{Y}_a^{11}(\omega) & -\mathbf{Y}_a^{12}(\omega) \\ \mathbf{0} & \mathbf{0} & \mathbf{Y}_b(\omega) \end{bmatrix} \times \begin{Bmatrix} \mathbf{F}_e(\omega) \\ \mathbf{F}_p(\omega) \\ \mathbf{F}_{ab}(\omega) \end{Bmatrix}. \tag{5}$$

We now introduce an inner product $\langle \mathbf{u},\mathbf{w} \rangle_{\mathbf{D}} = (\mathbf{D}\mathbf{u})^{\mathrm{H}}\mathbf{w}$ and its corresponding norm $\|\mathbf{u}\|_{\mathbf{D}}^2 = \langle \mathbf{u},\mathbf{u} \rangle_{\mathbf{D}}$ which will allow us to compactly express the vibratory power flows, where $\mathbf{u}$ and $\mathbf{w}$ are arbitrary complex vectors, $\mathbf{D}$ is any symmetric complex valued matrix, and the superscript H denotes the Hermitian of a vector. Due to the symmetry of $\mathbf{D}$, the norm possesses the following properties: $\mathrm{Re}(\|\mathbf{u}\|_{\mathbf{D}}^2) = \|\mathbf{u}\|_{\mathrm{Re}(\mathbf{D})}^2$ and $\mathrm{Im}(\|\mathbf{u}\|_{\mathbf{D}}^2) = -\|\mathbf{u}\|_{\mathrm{Im}(\mathbf{D})}^2$ where Re( ) and Im( ) are the real and imaginary part operators, respectively. The expression for the time-averaged transmitted power, P^t, is synthesized in the frequency domain from the interfacial forces and velocities via $(\omega/2\pi)\Sigma_k \int_0^{2\pi/\omega} \dot{q}_k(t) F_k(t)\,dt = \frac{1}{2}\mathrm{Re}(\langle \mathbf{v}(\omega),\mathbf{F}(\omega) \rangle_{\mathbf{I}})$. For each interface the power transmission equations take the form

$$P_e^t(\omega) = \tfrac{1}{2}\,\mathrm{Re}(\langle \mathbf{v}_e(\omega),\mathbf{F}_e(\omega) \rangle_{\mathbf{I}}) = \|\mathbf{F}_e(\omega)\|_{\mathbf{Q}_e(\omega)}^2, \tag{6a}$$

$$P_{pa}^t(\omega) = \tfrac{1}{2}\,\mathrm{Re}(\langle \mathbf{v}_{pa}(\omega),\mathbf{F}_p(\omega) \rangle_{\mathbf{I}}) = \|\mathbf{F}_e(\omega)\|_{\mathbf{Q}_{pa}(\omega)}^2, \tag{6b}$$

$$P_{ab}^t(\omega) = \tfrac{1}{2}\,\mathrm{Re}(\langle \mathbf{v}_{ab}(\omega),\mathbf{F}_{ab}(\omega) \rangle_{\mathbf{I}}) = \|\mathbf{F}_e(\omega)\|_{\mathbf{Q}_{ab}(\omega)}^2, \tag{6c}$$

where the effective mobilities, $\mathbf{Q}$, are as follows:

$$\mathbf{Q}_e(\omega) = \tfrac{1}{2}\,\mathrm{Re}(\mathbf{Y}_s^{11}(\omega) - \mathbf{Y}_s^{12}(\omega)\boldsymbol{\Gamma}_2(\omega)), \tag{6d}$$

$$\mathbf{Q}_{pa}(\omega) = \tfrac{1}{2}\,\mathrm{Re}(\boldsymbol{\Gamma}_2^{\mathrm{H}}(\omega)(\mathbf{Y}_a^{11}(\omega) - \mathbf{Y}_a^{12}(\omega)\boldsymbol{\Gamma}_1(\omega))\boldsymbol{\Gamma}_2(\omega)), \tag{6e}$$

$$\mathbf{Q}_{ab}(\omega) = \tfrac{1}{2}\,\mathrm{Re}((\boldsymbol{\Gamma}_1(\omega)\boldsymbol{\Gamma}_2(\omega))^{\mathrm{H}}\mathbf{Y}_b(\omega) \times (\boldsymbol{\Gamma}_1(\omega)\boldsymbol{\Gamma}_2(\omega))). \tag{6f}$$

Note that the transmitted powers are all quadratic forms of the excitation vector, $\mathbf{F}_e$, and the effective mobilities, $\mathbf{Q}$, describe how the excitation is filtered through the structure. They may also be expressed as quadratic forms of the free source velocity[12] by using the relation $\mathbf{v}_{sp}(\omega) = \mathbf{Y}_s^{21}(\omega)\mathbf{F}_e(\omega)$. Since design modifications change the input power as well as the transmitted power it is more convenient to present the ratio of transmitted to input power as a comparison quantity. These power ratios may be written as

$$\alpha_{pa}(\omega) = P_{pa}^t(\omega)/P_e^t(\omega) = \|\mathbf{F}_e(\omega)\|_{\mathbf{Q}_{pa}(\omega)}^2 / \|\mathbf{F}_e(\omega)\|_{\mathbf{Q}_e(\omega)}^2, \tag{7a}$$

$$\alpha_{ab}(\omega) = P_{ab}^t(\omega)/P_e^t(\omega) = \|\mathbf{F}_e(\omega)\|_{\mathbf{Q}_{ab}(\omega)}^2 / \|\mathbf{F}_e(\omega)\|_{\mathbf{Q}_e(\omega)}^2.$$

B. Modal approach

The modal synthesis procedure has been used previou to calculate the power flow in structures, but only for r joints.[4] The modal approach proposed here is divided two primary steps. The first of these, is to synthesize velocity field of the assembly from the component mod properties. In this step, any boundary conditions on the su assemblies may be used, e.g., fixed–fixed or fixed–fre though we opt to use free–free in the following derivati The second step is to treat the forced harmonic response the assembly as an externally applied velocity field and th to project the corresponding portions of this field onto ea subassembly with no other external constraints (i.e., wit free–free boundary conditions). The procedure is illustrate by first writing separately the equations of motion of t free–free source (s) and receiver (c) structures of Fig. 1(a

$$\mathbf{M}_s\ddot{\mathbf{q}}_s(t) + \mathbf{C}_s\dot{\mathbf{q}}_s(t) + \mathbf{K}_s\mathbf{q}_s(t) = \mathbf{L}_e^T\mathbf{F}_e(t), \tag{8}$$

$$\mathbf{M}_c\ddot{\mathbf{q}}_c(t) + \mathbf{C}_c\dot{\mathbf{q}}_c(t) + \mathbf{K}_c\mathbf{q}_c(t) = \mathbf{0}, \tag{8}$$

where $\mathbf{M}$, $\mathbf{C}$, and $\mathbf{K}$ are the mass, damping, and stiffn matrices, respectively, and $\mathbf{q}$ is the generalized displacem vector. Additionally $\mathbf{L}_e$ is a Boolean selection matrix wh extracts the excitation degrees-of-freedom from the sou degrees-of-freedom such that $\mathbf{F}_e(\omega)$ is the same vector h as in the mobility method. These quantities include all relevant degrees-of-freedom (such as n_s for the source, for the receiver) including those of the interior and in faces. Next we consider the modal decompositions of t structure assuming that the system mass, damping, and s ness matrices are symmetric and using the following v known modal orthogonality relations:

$$\boldsymbol{\Phi}_s^T\mathbf{M}_s\boldsymbol{\Phi}_s = \mathbf{I},$$

$$\boldsymbol{\Phi}_s^T\mathbf{C}_s\boldsymbol{\Phi}_s = \boldsymbol{\Xi}_s,$$

$$\boldsymbol{\Phi}_s^T\mathbf{K}_s\boldsymbol{\Phi}_s = \boldsymbol{\Lambda}_s,$$

$$\boldsymbol{\Phi}_c^T\mathbf{M}_c\boldsymbol{\Phi}_c = \mathbf{I},$$

$$\boldsymbol{\Phi}_c^T\mathbf{C}_c\boldsymbol{\Phi}_c = \boldsymbol{\Xi}_c,$$

$$\boldsymbol{\Phi}_c^T\mathbf{K}_c\boldsymbol{\Phi}_c = \boldsymbol{\Lambda}_c,$$

where $\boldsymbol{\Phi}$, $\boldsymbol{\Xi}$, and $\boldsymbol{\Lambda}$ are the system eigenvector, di damping, and eigenvalue matrices, respectively; se 1(c). Equation (9) may then be assembled in the parti form as follows, where the subscript z denotes the sub bly in the modal domain:

$$\boldsymbol{\Phi}_z = \begin{bmatrix} \boldsymbol{\Phi}_s & \mathbf{0} \\ \mathbf{0} & \boldsymbol{\Phi}_c \end{bmatrix},$$

$$\boldsymbol{\Xi}_z = \begin{bmatrix} \boldsymbol{\Xi}_s & \mathbf{0} \\ \mathbf{0} & \boldsymbol{\Xi}_c \end{bmatrix},$$

$$\boldsymbol{\Lambda}_z = \begin{bmatrix} \boldsymbol{\Lambda}_s & \mathbf{0} \\ \mathbf{0} & \boldsymbol{\Lambda}_c \end{bmatrix},$$

$$\mathbf{q}_z(\omega)=\begin{Bmatrix}\mathbf{q}_s(\omega)\\ \mathbf{q}_c(\omega)\end{Bmatrix}. \tag{10d}$$

We now need to integrate the joint dynamics into this formulation. Accordingly, the relative displacements across the joints/paths are given by

$$\boldsymbol{\delta}_p(\omega)=\mathbf{L}_z\mathbf{q}_z(\omega), \tag{11a}$$

$$\mathbf{L}_z=[\mathbf{L}_s,-\mathbf{L}_c], \tag{11b}$$

where the matrices $\mathbf{L}_s$ and $\mathbf{L}_c$ give the connectivities between the joint and the source and receiver, respectively, that is, they extract the interfacial degrees of freedom from the vector $\mathbf{q}_z$ which contains all the degrees of freedom of the assembly. To complete the assembly of the structure through the compliant joints, the following matrices are defined in the modal domain:

$$\mathbf{A}=\boldsymbol{\Lambda}_z+(\mathbf{L}_z\boldsymbol{\Phi}_z)^T\mathbf{K}_p(\mathbf{L}_z\boldsymbol{\Phi}_z), \tag{12a}$$

$$\mathbf{B}=\boldsymbol{\Xi}_z+(\mathbf{L}_z\boldsymbol{\Phi}_z)^T\mathbf{C}_p(\mathbf{L}_z\boldsymbol{\Phi}_z) \tag{12b}$$

along with its associated orthogonality relations: $\boldsymbol{\Psi}^T\boldsymbol{\Psi}=\mathbf{I}$; $\boldsymbol{\Psi}^T\mathbf{A}\boldsymbol{\Psi}=\boldsymbol{\Lambda}$; $\boldsymbol{\Psi}^T\mathbf{B}\boldsymbol{\Psi}=\boldsymbol{\Xi}$. The eigenvalues $\boldsymbol{\Lambda}$ of $\mathbf{A}$ are indeed the eigenvalues of the assembled structure and the corresponding assembly modes, $\boldsymbol{\Phi}$, are given by $\boldsymbol{\Phi}=\boldsymbol{\Phi}_z\boldsymbol{\Psi}$. This formulation assumes that the joint is proportionally damped such that both the component and assembly modes are real. For the assembled structure subjected to harmonic excitation of arbitrary amplitude $\mathbf{F}$ at frequency ω, the modal superposition with the use of the synthesis relations (12) yields the velocity response as

$$\begin{aligned}\mathbf{v}(\omega)&=i\omega\boldsymbol{\Phi}[\boldsymbol{\Lambda}-\omega^2\mathbf{I}+i\omega\boldsymbol{\Xi}]^{-1}\boldsymbol{\Phi}^T\mathbf{F}(\omega)\\&=i\omega\boldsymbol{\Phi}_z[\mathbf{A}-\omega^2\mathbf{I}+i\omega\mathbf{B}]^{-1}\boldsymbol{\Phi}_z^T\mathbf{F}(\omega),\end{aligned} \tag{13}$$

where $\mathbf{F}(\omega)=\{(\mathbf{L}_e^T\mathbf{F}_e(\omega))^T,\mathbf{0}^T\}^T$ and $\mathbf{v}(\omega)=\{\mathbf{v}_s^T(\omega),\mathbf{v}_c^T(\omega)\}^T$. This partitioning into the source $\mathbf{v}_s(\omega)$ and receiver components, $\mathbf{v}_c(\omega)$ continues as follows:

$$\mathbf{v}_s(\omega)=i\omega\boldsymbol{\Phi}_s\boldsymbol{\Psi}_s\boldsymbol{\Psi}^T[\mathbf{A}-\omega^2\mathbf{I}+i\omega\mathbf{B}]^{-1}\boldsymbol{\Phi}_z^T\mathbf{F}(\omega), \tag{14a}$$

$$\mathbf{v}_c(\omega)=i\omega\boldsymbol{\Phi}_c\boldsymbol{\Psi}_c\boldsymbol{\Psi}^T[\mathbf{A}-\omega^2\mathbf{I}+i\omega\mathbf{B}]^{-1}\boldsymbol{\Phi}_z^T\mathbf{F}(\omega), \tag{14b}$$

where $\boldsymbol{\Psi}_c$ are the rows of $\boldsymbol{\Psi}$ corresponding to the receiver degrees of freedom and $\boldsymbol{\Psi}_s$ are the rows of $\boldsymbol{\Psi}$ corresponding to the source degrees of freedom. From the assembly eigenvalue problem we know that $\boldsymbol{\Psi}^T\boldsymbol{\Psi}=\boldsymbol{\Psi}\boldsymbol{\Psi}^T=\mathbf{I}$ and thus $\boldsymbol{\Psi}_s\boldsymbol{\Psi}_s^T=\mathbf{I}$, $\boldsymbol{\Psi}_s\boldsymbol{\Psi}_c^T=\mathbf{0}$, $\boldsymbol{\Psi}_c\boldsymbol{\Psi}_s^T=\mathbf{0}$, and $\boldsymbol{\Psi}_c\boldsymbol{\Psi}_c^T=\mathbf{I}$. Utilizing these identities in the modal superposition, we find the source velocity field to be given by

$$\mathbf{v}_s(\omega)=i\omega\boldsymbol{\Phi}_s[\mathbf{I},\mathbf{0}][\mathbf{A}-\omega^2\mathbf{I}+i\omega\mathbf{B}]^{-1}\boldsymbol{\Phi}_z^T\mathbf{F}(\omega). \tag{15}$$

The matrix inversion can be performed in terms of submatrices[19] as in (3). After exploiting the fact that only the source is active, its velocity field may be stated as

$$\mathbf{v}_s(\omega)=i\omega\boldsymbol{\Phi}_s[\mathbf{I},\mathbf{0}]\begin{bmatrix}\boldsymbol{\Gamma}_4(\omega)\\ \boldsymbol{\Gamma}_3(\omega)\boldsymbol{\Gamma}_4(\omega)\end{bmatrix}\mathbf{F}_e(\omega), \tag{16a}$$

where the intermediate matrices are given by

$$\begin{aligned}\boldsymbol{\Gamma}_3(\omega)=&[\boldsymbol{\Lambda}_c-\omega^2\mathbf{I}+i\omega\boldsymbol{\Xi}_c+(\mathbf{L}_c\boldsymbol{\Phi}_c)^T(\mathbf{K}_p+i\omega\mathbf{C}_p)\\&\times(\mathbf{L}_c\boldsymbol{\Phi}_c)]^{-1}[(\mathbf{L}_s\boldsymbol{\Phi}_s)^T(\mathbf{K}_p+i\omega\mathbf{C}_p)(\mathbf{L}_c\boldsymbol{\Phi}_c)]^T,\end{aligned} \tag{16b}$$

$$\begin{aligned}\boldsymbol{\Gamma}_4(\omega)=&[(\boldsymbol{\Lambda}_s-\omega^2\mathbf{I}+i\omega\boldsymbol{\Xi}_s+(\mathbf{L}_s\boldsymbol{\Phi}_s)^T(\mathbf{K}_p+i\omega\mathbf{C}_p)\\&\times(\mathbf{L}_s\boldsymbol{\Phi}_s))-(\mathbf{L}_s\boldsymbol{\Phi}_s)^T(\mathbf{K}_p+i\omega\mathbf{C}_p)\\&\times(\mathbf{L}_c\boldsymbol{\Phi}_c)\boldsymbol{\Gamma}_3(\omega)]^{-1}(\mathbf{L}_c\boldsymbol{\Phi}_s)^T.\end{aligned} \tag{16c}$$

From above, it becomes apparent that although $\mathbf{v}_s$ is used which includes interior degrees-of-freedom, actually only the interface and excitation coordinates of the eigenvectors are needed, i.e., $\mathbf{L}_e\boldsymbol{\Phi}_s$, $\mathbf{L}_s\boldsymbol{\Phi}_s$, and $\mathbf{L}_c\boldsymbol{\Phi}_c$ if the multiplications with the Boolean matrices are done analytically. To pursue the power flow calculations, we next utilize the fact that the power dissipated in the entire structure equals the power input under steady-state conditions.

$$P^d(\omega)=\sum_k P_k^d(\omega)=P_e^I(\omega), \tag{17a}$$

$$P_e^I(\omega)=\tfrac{1}{2}\,\mathrm{Re}(\langle\mathbf{v}(\omega),\mathbf{F}(\omega)\rangle_1)=\|\mathbf{F}_e(\omega)\|^2_{\mathbf{R}_s(\omega)},$$

$$k=s,p,c \tag{17b}$$

$$\mathbf{R}_c(\omega)=-\tfrac{1}{2}\omega\,\mathrm{Im}((\mathbf{L}_e\boldsymbol{\Phi}_s)\boldsymbol{\Gamma}_4(\omega)). \tag{17c}$$

The power dissipated in the source component is given as follows by using (9) and (16):

$$P_s^d(\omega)=\tfrac{1}{2}\|\mathbf{v}_s(\omega)\|^2_{\mathbf{C}_s}=\|\mathbf{F}_e(\omega)\|^2_{\mathbf{R}_s(\omega)}, \tag{18a}$$

$$\mathbf{R}_s(\omega)=\tfrac{1}{2}\omega^2\,\mathrm{Re}(\boldsymbol{\Gamma}_4^{\mathrm{H}}(\omega)\boldsymbol{\Xi}_s\boldsymbol{\Gamma}_4(\omega)). \tag{18b}$$

Similarly for the receiver and joint, dissipated powers are

$$P_c^d(\omega)=\tfrac{1}{2}\|\mathbf{v}_c(\omega)\|^2_{\mathbf{C}_c}=\|\mathbf{F}_e(\omega)\|^2_{\mathbf{R}_c(\omega)}, \tag{19a}$$

$$P_p^d(\omega)=\tfrac{1}{2}\|\mathbf{L}_z\mathbf{v}(\omega)\|^2_{\mathbf{C}_p}=\|\mathbf{F}_e(\omega)\|^2_{\mathbf{R}_p(\omega)}, \tag{19b}$$

$$\mathbf{R}_c(\omega)=\tfrac{1}{2}\omega^2\,\mathrm{Re}((\boldsymbol{\Gamma}_3(\omega)\boldsymbol{\Gamma}_4(\omega))^{\mathrm{H}}\boldsymbol{\Xi}_c(\boldsymbol{\Gamma}_3(\omega)\boldsymbol{\Gamma}_4(\omega))), \tag{19c}$$

$$\mathbf{R}_p(\omega)=\frac{1}{2}\omega^2\,\mathrm{Re}\left\{\begin{bmatrix}\boldsymbol{\Gamma}_4(\omega)\\ \boldsymbol{\Gamma}_3(\omega)\boldsymbol{\Gamma}_4(\omega)\end{bmatrix}^{\mathrm{H}}(\mathbf{L}_z\boldsymbol{\Phi}_z)^T\mathbf{C}_p(\mathbf{L}_z\boldsymbol{\Phi}_z)\times\begin{bmatrix}\boldsymbol{\Gamma}_4(\omega)\\ \boldsymbol{\Gamma}_3(\omega)\boldsymbol{\Gamma}_4(\omega)\end{bmatrix}\right\}. \tag{19d}$$

As with the mobility method, the power equations are quadratic forms of the excitation. But now the power dissipated in the receiving (and/or source) structure can be broken down into its modal contributions

$$P_c^d(\omega)=\sum_r P_{c,r}^d(\omega), \tag{20a}$$

$$P_{c,r}^d(\omega)=\zeta_r\omega_r|\omega G_r(\omega)|^2, \tag{20b}$$

where $P_{c,r}^d(\omega)$ is the power dissipated by each mode of the receiving structure, ζ_r is the damping ratio of the rth mode, ω_r is the natural frequency of the rth mode, and G_r is the rth element of the vector $\boldsymbol{\Gamma}_3\boldsymbol{\Gamma}_4\mathbf{F}_e$. Similarly the power dissipated

within the entire assembly (17) may be expressed in terms of the assembly modes, $\mathbf{\Phi}$, as

$$P^d(\omega)=\tfrac{1}{2}\|\mathbf{v}(\omega)\|_{\mathbf{C}}^2=\|\mathbf{F}_c(\omega)\|_{\mathbf{R}(\omega)}^2 \tag{21a}$$

$$\mathbf{R}(\omega)=\tfrac{1}{2}\omega^2\ \mathrm{Re}((((\mathbf{\Lambda}-\omega^2\mathbf{I}+i\omega\mathbf{\Xi})^{-1}\mathbf{\Phi}_e^T)^H\mathbf{\Xi}((\mathbf{\Lambda}-\omega^2\mathbf{I}+i\omega\mathbf{\Xi})^{-1}\mathbf{\Phi}_e^T)), \tag{21b}$$

where $\mathbf{\Phi}_e$ is a matrix whose rows contain the excitation degrees-of-freedom for each assembly mode. These equations permit us to calculate the following structural modal dissipation efficiencies $\sigma(\omega)$ analogous to the modal radiation efficiencies which are in common usage in the discipline of acoustics.[22]

$$\sigma_{s,r}(\omega)=P^d_{s,r}(\omega)/P^t_e(\omega),\quad r\in[1,n_s], \tag{22a}$$

$$\sigma_{c,r}(\omega)=P^d_{c,r}(\omega)/P^t_e(\omega),\quad r\in[1,n_c], \tag{22b}$$

$$\sigma_{p,k}(\omega)=P^d_{p,k}(\omega)/P^t_e(\omega),\quad k\in[1,n_p], \tag{22c}$$

$$\sigma_{z,r}(\omega)=P^d_{z,r}(\omega)/P^t_e(\omega),\quad r\in[1,n_z]; \tag{22d}$$

where $n_z=n_s+n_c$. The equation for the joint dissipation efficiency (22c) is not truly a modal efficiency (since the massless joint has no modes), rather it is the efficiency of the various joint paths to dissipate power.

C. Relationship between mobility and modal approaches

Whereas with the mobility approach the emphasis was on the transmitted power, P^t, between components, with the modal approach the emphasis is on the dissipated power, P^d, in each component. Therefore, unlike the mobility approach, the modal approach requires detailed information about the internal dynamics of a structure and hence it is much larger in dimension. The two methods are otherwise related by the power balance equation $P^d(\omega)=P^t_{\mathrm{in}}(\omega)-P^t_{\mathrm{out}}(\omega)$ which states that the difference between the power transmitted into, $P^t_{\mathrm{in}}(\omega)$, and out of a structure, $P^t_{\mathrm{out}}(\omega)$, equals the power dissipated in that structure at any ω under the steady-state conditions.

Furthermore, the two proposed methods are complementary in nature. The mobility method is particularly suited to the efforts of reducing the power which is transmitted by the joints/paths (as if they were treated as isolators); this is analogous to trying to achieve as high of a mobility (or impedance) mismatch as possible. However, since not all joints lend themselves to be ideal isolators, inevitably some power will leak into the receiver to be dissipated therein. Investigating how this power is dissipated within the receiver is the strength of the modal approach. Therefore the two methods in conjunction with one another may be used to study the noise control problem of which paths transmit the most power to the receiver and which modes of the receiver most effectively dissipate that power.

One of the benefits of the mobility approach is the variety of methods by which the structural mobilities can be obtained. For instance, the appropriate elements of the equation

$$Y^{mn}(\omega)=i\omega[(\mathbf{K}-\omega^2\mathbf{M}+i\omega\mathbf{C})^{-1}]^{mn} \tag{23}$$

may be used where the superscript mn refers to the ele (m,n) of the matrix; it is this procedure which is use quantify the compliant joint mobilities (with the mass ma elements set to zero, since the joints are considered m less). The modal decomposition of this equation may also utilized which takes on the following form:

$$Y^{mn}(\omega)=i\omega\sum_r\ \frac{\phi_{r,m}\phi_{r,n}}{(\omega_r^2-\omega^2)+i\omega(2\zeta_r\omega_r)},$$

where the modal properties can be obtained via analytic experimental,[14] or finite element procedures. Note that assumes proportional damping for the structure.

II. RESULTS

A. Discrete system example

To illustrate the proposed methods, a principal exam of Fig. 2 is chosen since exact results for a subset of t configuration have appeared in the literature.[4] This syste of dimension $5n$, where n may be chosen arbitrarily, inc porates many of the features which we intend to exami with our methods, e.g., multiple compliant joints and co pliant foundation. In the assembly, upper (#4) and lower (joints consist of both stiffness and damping matrices of mension n and two parallel paths are clearly seen. The str ture also has a compliant foundation/termination (#1) wh acts as an energy sink. For the sake of simplicity, onl single excitation is considered in this study although methods are capable of handling multiple excitations wit the source structure. The system matrices are given as f lows in matrix form:

$$\mathbf{M}_s=\mathrm{diag}[\mathbf{M}_4,\mathbf{M}_5],$$

$$\mathbf{K}_s=\begin{bmatrix}\mathbf{K}_5 & -\mathbf{K}_5\\ -\mathbf{K}_5 & \mathbf{K}_5\end{bmatrix},$$

$$\mathbf{C}_s=\begin{bmatrix}\mathbf{C}_5 & -\mathbf{C}_5\\ -\mathbf{C}_5 & \mathbf{C}_5\end{bmatrix},$$

$$\mathbf{M}_a=\mathrm{diag}[\mathbf{M}_1,\mathbf{M}_2,\mathbf{M}_3],$$

$$\mathbf{K}_a=\begin{bmatrix}\mathbf{K}_2 & -\mathbf{K}_2 & \mathbf{0}\\ -\mathbf{K}_2 & \mathbf{K}_2+\mathbf{K}_3 & -\mathbf{K}_3\\ \mathbf{0} & -\mathbf{K}_3 & \mathbf{K}_3\end{bmatrix},$$

$$\mathbf{C}_a=\begin{bmatrix}\mathbf{C}_2 & -\mathbf{C}_2 & \mathbf{0}\\ -\mathbf{C}_2 & \mathbf{C}_2+\mathbf{C}_3 & -\mathbf{C}_3\\ \mathbf{0} & -\mathbf{C}_3 & \mathbf{C}_3\end{bmatrix},$$

$$\mathbf{K}_p=\mathrm{diag}[\mathbf{K}_4,\mathbf{K}_6],$$

$$\mathbf{C}_p=\mathrm{diag}[\mathbf{C}_4,\mathbf{C}_6],$$

$$\mathbf{K}_b=\mathbf{K}_1,$$

$$\mathbf{C}_b=\mathbf{C}_1,$$

and for the modal approach the connectivity matrices ar

$$\mathbf{L}_c=[\mathbf{I},\mathbf{0}],$$

$$\mathbf{L}_s=\mathrm{diag}[\mathbf{I},\mathbf{I}],$$

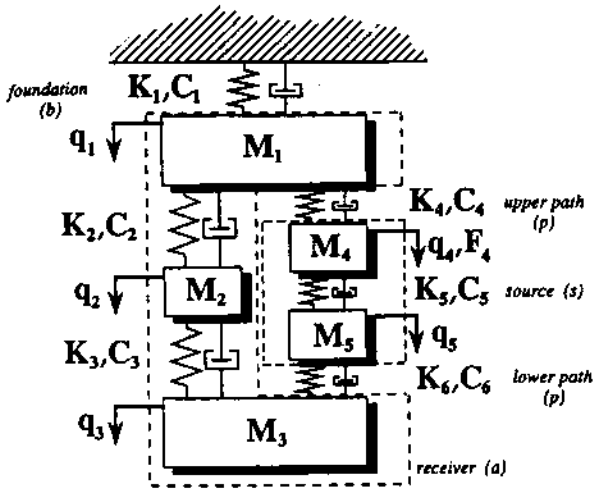

FIG. 2. Schematic of lumped parameter model. All quantities are matrices or vectors of dimension n.

$$\mathbf{L}_c=\begin{bmatrix}\mathbf{I} & \mathbf{0} & \mathbf{0}\\ \mathbf{0} & \mathbf{0} & \mathbf{I}\end{bmatrix}, \tag{26c}$$

$$\mathbf{L}_b=[\mathbf{I},\ \mathbf{0},\ \mathbf{0}], \tag{26d}$$

$$\mathbf{K}_c=\mathbf{K}_a=\mathrm{diag}[\mathbf{K}_1,\mathbf{0},\mathbf{0}], \tag{26e}$$

$$\mathbf{C}_c=\mathbf{C}_a+\mathrm{diag}[\mathbf{C}_1,\mathbf{0},\mathbf{0}], \tag{26f}$$

$$\mathbf{M}_c=\mathbf{M}_a, \tag{26g}$$

where $\mathbf{L}_e$ selects the excitation degrees-of-freedom, $\mathbf{L}_s$ selects the joint interface coordinates of the source structure, $\mathbf{L}_c$ selects the joint interface coordinates of the receiver structure, while $\mathbf{L}_b$ selects the foundation coordinates of the receiver structure.

We now consider both of the proposed approaches. Using Eq. (23), we obtain the following mobility matrices of each component with reference to Fig. 2:

$$\mathbf{Y}_s(\omega)=i\omega\begin{bmatrix}\mathbf{L}_e\\ \mathbf{L}_s\end{bmatrix}[\mathbf{K}_s-\omega^2\mathbf{M}_s+i\omega\mathbf{C}_s]^{-1}\begin{bmatrix}\mathbf{L}_e\\ \mathbf{L}_s\end{bmatrix}^T, \tag{27a}$$

$$\mathbf{Y}_a(\omega)=i\omega\begin{bmatrix}\mathbf{L}_c\\ \mathbf{L}_b\end{bmatrix}[\mathbf{K}_a-\omega^2\mathbf{M}_a+i\omega\mathbf{C}_a]^{-1}\begin{bmatrix}\mathbf{L}_c\\ \mathbf{L}_b\end{bmatrix}^T, \tag{27b}$$

$$\mathbf{Y}_p(\omega)=i\omega[\mathbf{K}_p+i\omega\mathbf{C}_p]^{-1}, \tag{27c}$$

$$\mathbf{Y}_b(\omega)=i\omega[\mathbf{K}_b+i\omega\mathbf{C}_b]^{-1}, \tag{27d}$$

where each of the submatrices in (26) and (27) are of dimension n. These properties in conjunction with Eqs. (18) and (19) from Sec. II C yield the power dissipated in each component. The transmitted powers can be obtained from the power balance equations (Sec. II C) as mentioned earlier, e.g., $P^t_{pc}(\omega)=P^d_c(\omega)$.

B. Case studies

1. Scalar joints

Using the expressions (25) in the synthesis procedure (6) and (7), we now investigate the power flows between the components initially for the case $n=1$, using the following parameters: $\mathbf{M}_1=5\cdot m$, $\mathbf{M}_2=3\cdot m$, $\mathbf{M}_3=m$, $\mathbf{M}_4=m$, $\mathbf{M}_5=2\cdot m$;

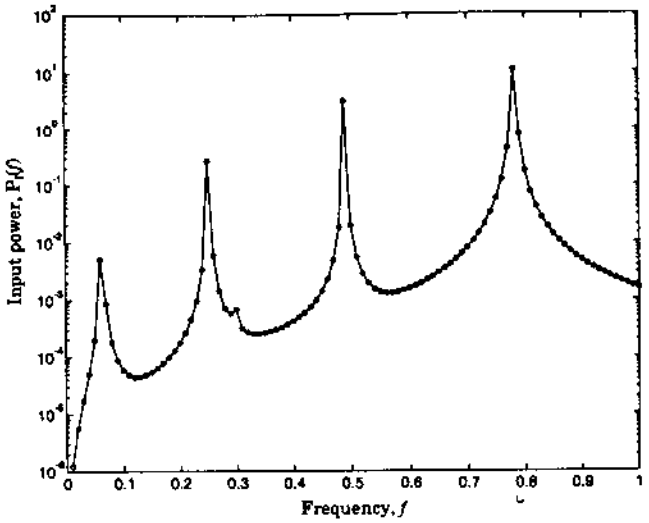

FIG. 3. Comparison of input power for the lumped parameter model ($n=1$) using different approaches. ——— exact (unsynthesized); ○○○○ mobility-based synthesis.

$\mathbf{K}_1=2\cdot k$, $\mathbf{K}_2=4\cdot k$, $\mathbf{K}_3=2\cdot k$, $\mathbf{K}_4=10\cdot k$, $\mathbf{K}_5=10\cdot k$, $\mathbf{K}_6=5\cdot k$, where m and k are arbitrary; and $\mathbf{C}_\mu=\eta\mathbf{K}_\mu$ for $\mu=1,\ldots,6$. In Fig. 3 we show the comparison of the input power flow using the exact (unsynthesized) and proposed (synthesized) mobility and modal methods. Here the frequency scale f can be viewed as dimensionless given $m=k=1$. The excellent matches are to be expected since our synthesis procedure, like others,[4] is exact when the full modal basis, or all the degrees of freedom, are included. For our system, there exist thermodynamic limits on the power flows, i.e., $P^t_e(\omega)>P^t_{pa}(\omega)>P^t_{ab}(\omega)$ or $\alpha_{ab}(\omega)<\alpha_{pa}(\omega)<1$ due to the fact that all of the components besides the source are passive. If we now use the power ratios, α, to study the power flows through the joint paths as in Fig. 4, we note a peculiar occurrence; the power flow through the upper joint is greater than one which may seen to violate the earlier thermodynamic considerations. Nonetheless, although the upper joint

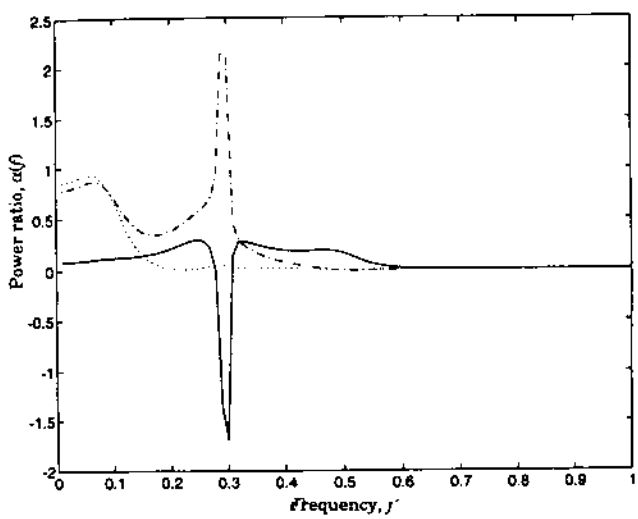

FIG. 4. Power ratios for the lumped parameter model ($n=1$). ——— α_{pa} (lower path); – · – · α_{pa} (upper path); and · · · · α_{ab}.

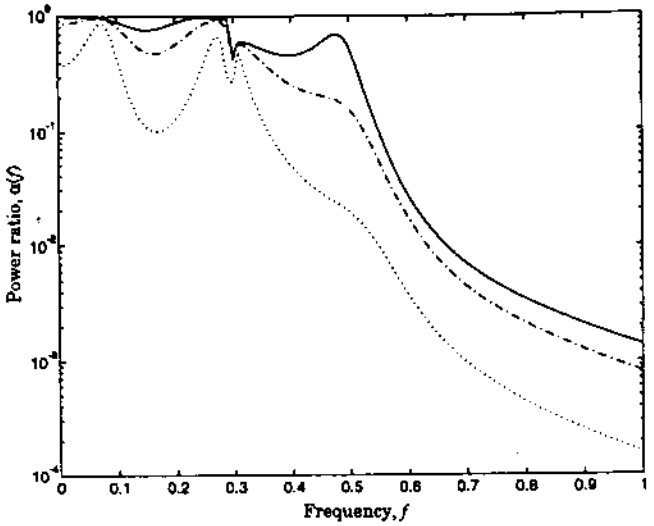

FIG. 5. Effect of joint damping on the transmitted power of the lumped parameter model ($n=1$). ——— $\eta=10^{-4}$; –·–· $\eta=10^{-3}$; and ···· $\eta=10^{-2}$.

power ratio exceeds one, the net joint/path power ratio is less than one, so that the thermodynamic conditions are indeed satisfied.

Next, one can consider some damping studies using the mobility approach. Figure 5 shows the effect of altering the joint dissipation characteristics. Increasing the joint damping only has large effect on the power transmitted in the frequency regime where there is reasonably large relative displacement across the joint. This is further examined in Fig. 6 where large $\sigma_{p,k}$ values show frequencies at which the joint dynamics are dominant; at $f=0.5$ the lower joint dissipates the most significant portion of the power, while the upper joint never dissipates more than 50% of the power.

Whereas the advantage of the mobility approach is its reduced dimension, the advantage of the modal approach is the ability to study structural modal dissipation efficiencies (22). This capability is demonstrated in Fig. 7. When investigating the efficiencies of the assembly modes [Fig. 7(a),(c)]

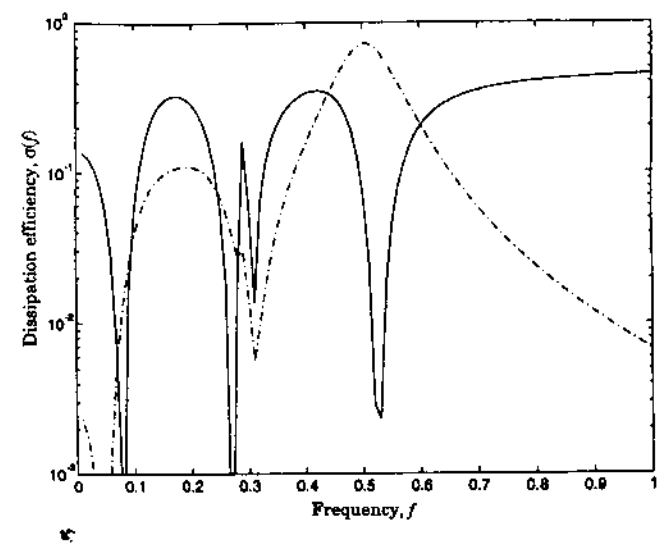

FIG. 6. Dissipation efficiencies of the joints for the lumped parameter model ($n=1$). ——— $\sigma_{p,1}$ (upper path); –·–· $\sigma_{p,2}$ (lower path).

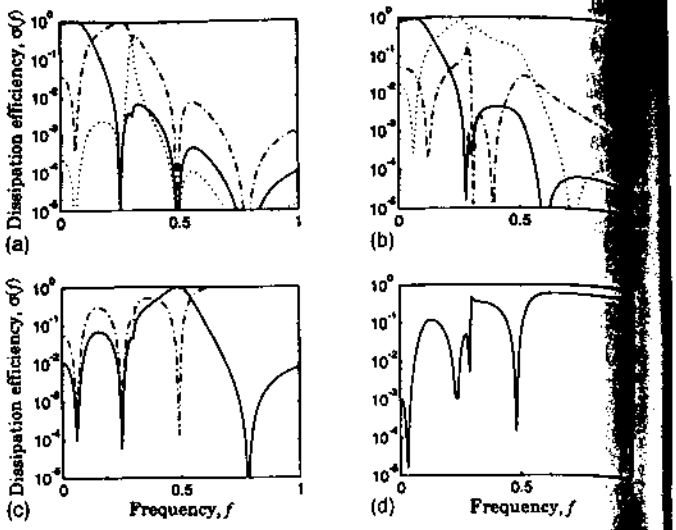

FIG. 7. Modal dissipation efficiencies for the lumped parameter model ($n=1$). (a) For the assembly modes. ——— $\sigma_{z,1}$; –·–· $\sigma_{z,2}$; and ···· $\sigma_{z,3}$. (b) For the receiver component modes. ——— $\sigma_{c,1}$; –·–· $\sigma_{c,2}$; and ···· $\sigma_{c,3}$. (c) For the assembly modes. ——— $\sigma_{z,4}$; –·–· $\sigma_{z,5}$. (d) For the source component modes. --- $\sigma_{s,2}$.

at a frequency which coincides with a natural frequency, one notes that most of the power is dissipated by the assembly mode which corresponds to this natural frequency. The assembly modal dissipation efficiencies will have only a single peak occurring at its corresponding natural frequency. Also one may note that some modes do not dissipate much power, for example modes whose nodes (antiresonances) coincide with one or more excitation locations contribute significantly less to the power dissipation. However, since we are interested in suggesting modifications to the components, we should also investigate the component modal dissipation efficiencies as given by Eq. (22); Fig. 7(b) and (d) show these results side by side with the assembly response for the sake of comparison. The rigid body mode of the semidefinite source component has no contribution to the dissipated power since it has no strain energy (or relative displacement) associated with it. Similarly, modifications to the joint damping should have the largest effect near the 4th natural frequencies of the assembly since they correspond to the modes with the most significant relative displacements across the lower joint.

2. Vector joints

Vector paths are simulated next by setting $n=2$ in Eqs. (25)–(27) and using the following system matrices:

$$\mathbf{M}_1=5\mathbf{I}_2, \tag{28a}$$

$$\mathbf{M}_2=3\mathbf{I}_2, \tag{28b}$$

$$\mathbf{M}_3=1\mathbf{I}_2, \tag{28c}$$

$$\mathbf{M}_4=1\mathbf{I}_2, \tag{28d}$$

$$\mathbf{M}_5=2\mathbf{I}_2, \tag{28e}$$

$$\mathbf{K}_1=2\mathbf{S}, \tag{28f}$$

$$\mathbf{K}_2=4\mathbf{S}, \tag{28g}$$

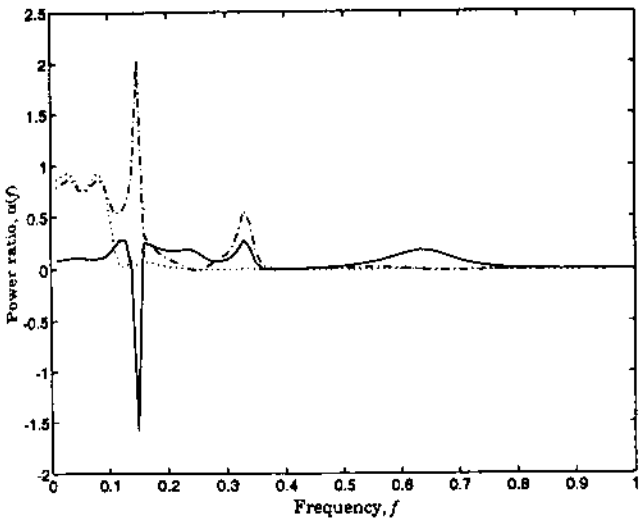

FIG. 8. Power ratios for the lumped parameter model ($n=2$). ——— α_{pa} (lower path); –·–· α_{pa} (upper path); and ····· α_{ab}.

$$\mathbf{K}_3 = 2\mathbf{S}, \tag{28h}$$

$$\mathbf{K}_4 = 10\mathbf{S}, \tag{28i}$$

$$\mathbf{K}_5 = 10\mathbf{S}, \tag{28j}$$

$$\mathbf{K}_6 = 5\mathbf{S}, \tag{28k}$$

where

$$\mathbf{S} = \begin{bmatrix} 1.00 & 0.75 \\ 0.75 & 1.00 \end{bmatrix} \tag{28l}$$

and $\mathbf{1}_2$ is the 2×2 identity matrix. Figure 8 shows the power ratios for the upper and lower path as well as for the foundation path. Again we note that as in Fig. 4, the power ratios through each path may exceed one, but their sum must be less than one. Increasing the joint damping has the effect of reducing the transmitted power ratio as revealed by Fig. 9. An increase of the joint damping factor by an order of magnitude (from $\eta=0.001$ to $\eta=0.010$) causes the power ratio to decrease by an order of magnitude at the higher frequencies.

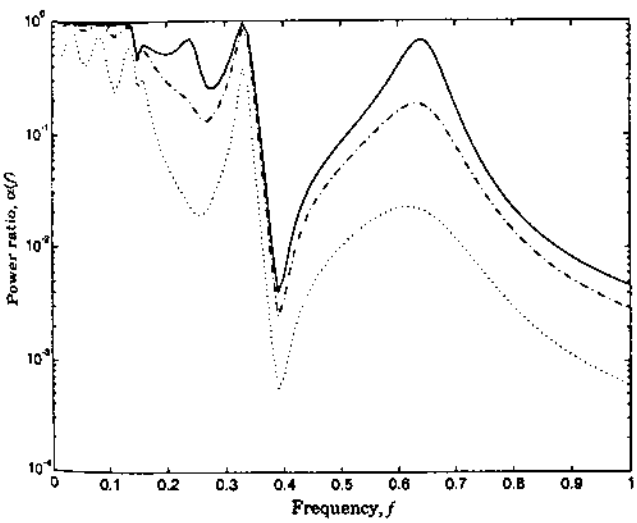

FIG. 9. Effect of joint damping on the transmitted power for the lumped parameter model ($n=2$). ——— $\eta=10^{-4}$; –·–· $\eta=10^{-3}$; and ····· $\eta=10^{-2}$.

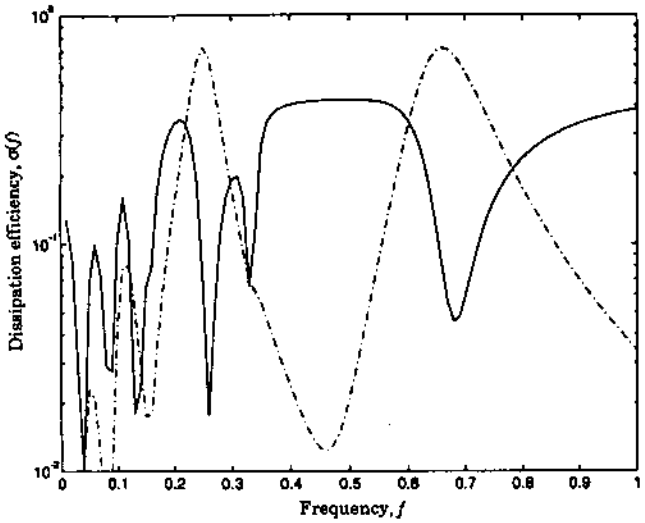

FIG. 10. Dissipation efficiencies of the joints for the lumped parameter model ($n=2$). ——— $\sigma_{p,1}+\sigma_{p,2}$ (upper path); –·–· $\sigma_{p,3}+\sigma_{p,4}$ (lower path).

In order to distinguish the frequencies at which the joint become active, Fig. 10 shows the dissipation efficiencies of the upper and lower paths. There exist two frequencies at which the lower joint dissipates the majority (70%) of the assembly's power; incidentally, it is at these frequencies that the joint dissipation had the most effect in Fig. 9. Dissipation efficiencies of selected assembly and component modes, as shown in Fig. 11, show trends similar to those of Fig. 7. Again the receiver modes are most efficient at low frequencies while the (nonrigid) source modes dominate at the higher frequencies. This seems consistent with continuous systems in which high frequency energy fails to escape the structural near-field. Also noteworthy from a design aspect is that the dissipation of the 6th and 9th assembly modes can be attributed mostly to the 6th receiver mode. This result can

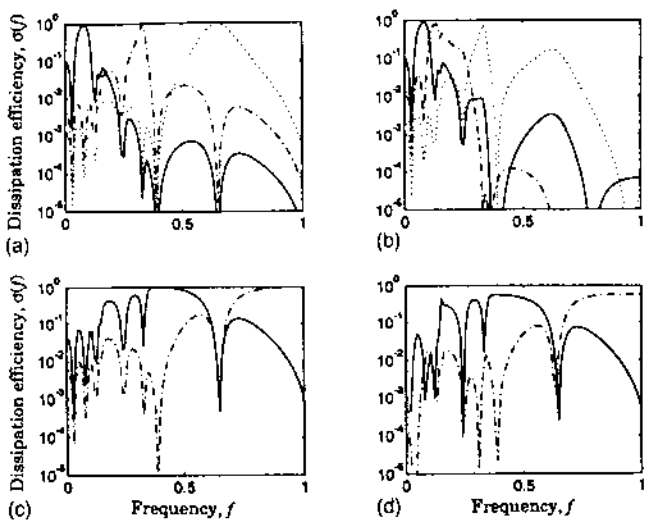

FIG. 11. Modal dissipation efficiencies for the lumped parameter model ($n=2$). (a) For the assembly modes. ——— $\sigma_{z,2}$; –·–· $\sigma_{z,6}$; and ····· $\sigma_{z,9}$. (b) For the receiver component modes. ——— $\sigma_{c,2}$; –·–· $\sigma_{c,4}$; and ····· $\sigma_{c,6}$. (c) For the assembly modes. ——— $\sigma_{z,7}$; –·–· $\sigma_{z,10}$. (d) For the source component modes. ——— $\sigma_{s,3}$; –·–· $\sigma_{s,4}$.

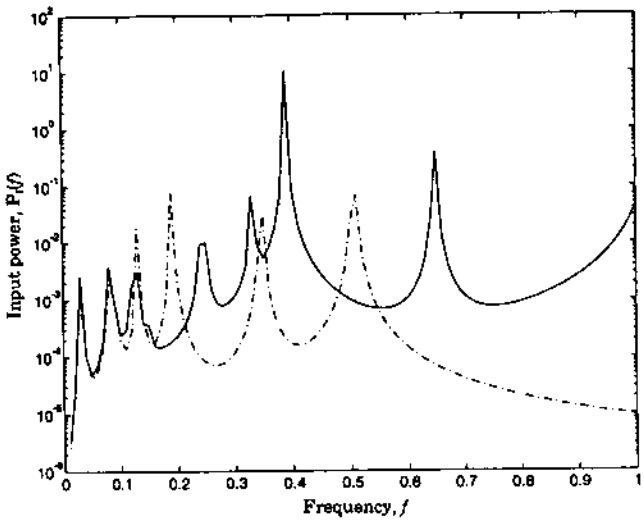

FIG. 12. Investigation of effect of joint compliance on input power for the lumped parameter model ($n=2$). ——— compliant joints; – · – rigid joints.

simplify design modifications by allowing the designer to concentrate on a particular component mode rather than multiple assembly modes.

In the next set of figures the importance of properly modeling the joints is demonstrated. Figure 12 shows the difference in the response for rigid and compliant joints. The system with compliant joints has ten natural frequencies while the system with rigid joints has only six natural frequencies (since $\mathbf{q}_1=\mathbf{q}_4$ and $\mathbf{q}_3=\mathbf{q}_5$). For frequencies greater than 0.1, the difference becomes quite significant. In any structure, these differences become pronounced in the frequency range where there is significant displacements across the joints. Not only is the compliance of the joint important but so is the dimensionality of the joint. The effect of modeling the joints as scalar rather than vector paths is shown in Fig. 13. For the $n=2$ case, we will refer to the first degree of freedom at each node as the primary degree of freedom, and

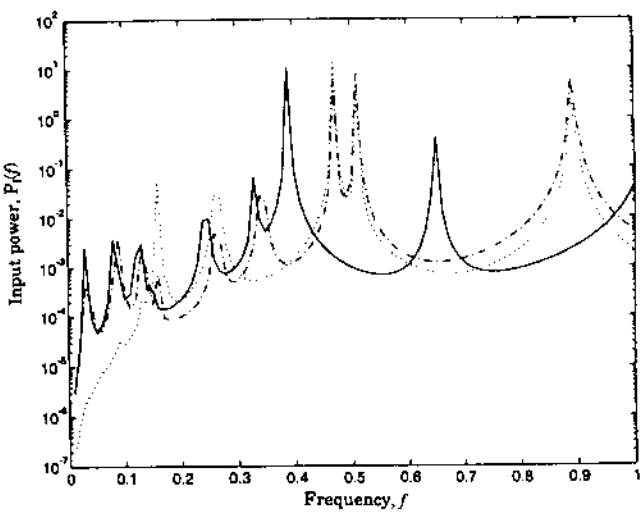

FIG. 13. Investigation of effect of neglecting vector path in joint on input power for the lumped parameter model ($n=2$). ——— vector path; – · – · only first scalar path included in both joints; · · · · only second scalar path included in both joints. Dimension of scalar path is 1, dimension of vector path is 2.

to the second degree of freedom as the secondary degr freedom; the excitation is only applied to the primary d of freedom at the fourth node. It should be noted that the primary degrees of freedom are retained in the joints response reasonably matches the exact solution for low quencies ($f<0.2$). However, when only the secondary grees of freedom are retained, the discrepancy is ext over the entire frequency range.

III. CONCLUSION

Refinements to two existing methods have been in duced which allow one to study the effects of joints on structure-borne power flow at low frequencies. Each o proposed methods has its own unique emphasis or appl tion. For example, the mobility method focuses on w path transmits the most power between structures. Howe the modal method emphasizes which structural mode di pates the most power once it is transmitted into a partic structure. Furthermore, the importance of properly mode the joint properties (e.g., their compliance and dimensi has been demonstrated. Also the importance of the j damping has been investigated; this is of practical impor tance since in a builtup assembly much of the damping may be attributed to the joints.

Interestingly, the proposed modal method has many parallels with other analysis methods; see Ref. 22 for a review. A comparative study of various methods is clearly beyond the scope of this paper, however a few qualitative observations are as follows. For example, Eq. (23b) for the narrowband analysis appears to be similar to the broadband statistical energy analysis (SEA) assumption that power dissipated is proportional to the system energy content. Woodhouse[23] further extended the SEA analogy to heat transfer, and equated thermal capacity to modal density and radiative loss to damping. A similar but not identical relation can be seen from Eq. (23b), when one notes that the absolute value term $|G_r|^2$, is equivalent to the component's modal kinetic energies, and $2\zeta_r\omega_r$ is equivalent to the modal loss factor.

Finally, it should be pointed out that the proposed analysis methods are exact only when one possesses the entir modal basis. However for any realistic structure, the moda basis must be truncated at some finite number. In particular the use of free–free boundary conditions makes the propose methods somewhat susceptible to these modal truncation Consequently, modal truncation/dynamic reduction issue need to be addressed since they are believed to be critical i the successful implementation of the methods to practic problems which may range from sheet metal structures t rotating equipment.

ACKNOWLEDGMENT

This work has been supported by the U.S. Army R search Office [URI Grant No. DAAL-03-92-G-0120; Proje Monitor: Dr. T. L. Doligalski].

[1] R. C. N. Leung and R. J. Pinnington, "Wave propagation through rig angled joints with compliance-flexural incident wave," J. Sound V 142(1), 31–46 (1990).
[2] R. C. N. Leung and R. J. Pinnington, "Wave propagation through rig

angled joints with longitudinal incidence wave," J. Sound Vib. **153**(2), 223–237 (1992).
[3] R. J. Pinnington and R. G. White, "Power flow through machine isolators to resonant and non-resonant beams," J. Sound Vib. **75**(1), 179–197 (1981).
[4] J. E. Farstad and R. Singh, "Structurally transmitted power in discretely joined damped component assemblies," J. Acoust. Soc. Am. **97**, 2855–2865 (1995).
[5] J. M. Cushieri, "Vibration transmission through periodic structures using a mobility power flow approach," J. Sound. Vib. **143**(1), 65–74 (1990).
[6] J. M. Cushieri, "Parametric analysis of the power flow on an L-shaped plate using a mobility power flow approach," J. Acoust. Soc. Am. **91**, 2686–2695 (1990).
[7] B. A. T. Petersson, "Structural acoustic power transmission by point moment and force excitation, part I: beam- and frame-like structures," J. Sound Vib. **160**(1), 43–66 (1993).
[8] B. A. T. Petersson, "Structural acoustic power transmission by point moment and force excitation, part II: plate-like structures," J. Sound Vib. **160**(1), 67–91 (1993).
[9] A. H. Nayfeh, A. F. Vakakis, and T. A. Nayfeh, "A method for analyzing the interaction of nondispersive structural waves and nonlinear joints," J. Acoust. Soc. Am. **93**, 849–856 (1993).
[10] H. G. D. Goyder and R. G. White, "Vibrational power flow into built-up structures, part I: introduction and approximate analyses of beam and plate-like foundations," J. Sound Vib. **68**(1), 59–75 (1980).
[11] S. Ljungren, "Transmission of structure-borne sound from a beam into an infinite plate," J. Sound. Vib. **100**(3), 309–320 (1985).
[12] J. M. Mondot and B. Petersson, "Characterization of structure-borne sound sources: the source descriptor and the coupling function," J. Sound Vib. **114**(3), 507–518 (1985).
[13] B. Petersson and J. Plunt, "On effective mobilities in the prediction of structure-borne sound transmission between a source structure and a receiving structure, part I: theoretical background and basic experimental studies," J. Sound Vib. **82**(4), 517–529 (1982).
[14] D. D. Kana and L. M. Vargas, "Transient excitation and mechanical admittance test techniques for prediction of payload vibration environments," NASA CR-2787 (1977).
[15] Y. Ren and C. F. Beards, "On the nature of FRF joint identification technique," Proc. 11th IMAC, 473–478 (1993).
[16] A. Simpson, "A generalization of Kron's eigenvalue procedure," J. Sound Vib. **26**(1), 129–139 (1973).
[17] D. V. Wright, "Impedance analysis of distributed mechanical systems," ASME Colloquium on Mechanical Impedance Methods for Mechanical Vibrations, 19–42 (1958).
[18] H. J. Carlin and A. B. Giordano, *Network Theory: An Introduction to Reciprocal and Non-reciprocal Circuits* (Prentice-Hall, Englewood Cliffs, NJ, 1964).
[19] S. Rubin, "Transmission matrices for vibration and their relation to admittance and impedance," ASME J. Eng. Ind. 9–21 (1964).
[20] B. A. T. Petersson and B. M. Gibbs, "Use of the source descriptor concept in studies of multi-point and multi-directional vibrational sources," J. Sound Vib. **168**(1), 157–176 (1993).
[21] R. J. Pinnington, "Using the envelope of the frequency response in the measurement of power absorbed by a finite structure," J. Sound Vib. **109**(1), 127–139 (1986).
[22] J. E. Farstad, M. R. Lee, and R. Singh, "Analysis of structure-borne and radiated sound using component modal bases," Appl. Acoust. **43**, 217–246 (1994).
[23] J. Woodhouse, "An introduction to statistical energy analysis of structural vibration," Appl. Acoust. **14**, 455–469 (1981).